FLiPASED
WWW.FLIPASED.EU

D2.3 Analytical Redundancy Methods

Balint Patartics (SZTAKI), Matthias Wuestenhagen (DLR), Peter Bauer (SZTAKI), Balint Vanek (SZTAKI)

GA number:	815058
Project acronym:	FLIPASED
Project title:	FLIGHT PHASE ADAPTIVE AEROSERVO-ELASTIC AIRCRAFT DESIGN METHODS
Funding Scheme: H2020	**ID:** MG-3-1-2018
Latest version of Annex I:	1.1 released on 12/04/2019
Start date of project: 01/09/2019	**Duration:** 40 Months

Lead Beneficiary for this deliverable:	SZTAKI
Last modified: 24/08/2021	**Status:** Delivered
Due date: 20/08/2021	

Project co-ordinator name and organisation:	Bálint Vanek, SZTAKI
Tel. and email: **+36 1 279 6113**	vanek@sztaki.hu
Project website:	www.flipased.eu

“This document is part of a project that has received funding from the European Union’s Horizon 2020 research and innovation programme under grant agreement No 815058.”

Dissemination Level		
PU	Public	X
CO	Confidential, only for members of the consortium (including the Commission Services)	

Glossary

FDI	Fault detection and isolation
GLA	Gust load alleviation
LTI	Linear time invariant
MM	Multiple-model
MMAC	Multiple-model adaptive control
WRBM	Wing root bending moment

Table of contents

List of Figures

1 Executive Summary

The goal of this deliverable was to explore analytical redundancy methods for fault tolerance of the FLiPASED aircraft providing Fault Detection and Isolation (FDI) and sensor-actuator selection. However, as the aircraft is designed to test flexible wings with active control for flutter suppression and it is propelled with liquid fuel the effects of flexibility and the continuously changing mass can not be neglected. Thus first, the effect of flexibility on actuator and sensor fault detection design is examined and then the effect of the changing mass in gust load alleviation control design is explored.

One of the challenges in designing a FDI system for a flexible aircraft is to obtain an appropriate flexible model of it as opposed to rigid aircraft where modelling (or identification) is more traditional. Such a model is in general more complex and its construction requires special expertise. The report demonstrates that fast and accurate FDI for the FLiPASED aircraft indeed necessitates the use of a flexible model but if the performance criteria can be relaxed and the sensor configuration can be changed, a rigid aircraft model can also be sufficient. H_∞ synthesis is used to design filters that detect the fault of the elevator actuator and the angle of attack sensor. Various sensor configurations and bandwidth specifications are used to compare the performance of the rigid and the flexible model-based designs.

Within the FliPASED project a multiple-model adaptive gust load alleviation (GLA) control system for the demonstrator aircraft is discussed and synthesised to solve the issue of increased vulnerability of modern aircraft configurations to gust encounters. Multiple-model adaptive control allows to identify the controller suiting best the aircraft's current properties like mass distribution by means of model detection methods. Different mass cases of the FliPASED demonstrator aircraft are considered by artificially attaching masses to the structural model. For each mass case a gust load alleviation controller is synthesized. Thus, a new control design approach is presented and applied to the demonstrator aircraft. Thereby, the advantages and challenges of the multiple-model adaptive control technique using methods inspired by fault detection, isolation and recovery in the context of the operation and design process of flexible aircraft can be discussed.

2 Fault detection

The purpose of Fault Detection and Isolation (FDI) is to develop tools with which faulty behaviour of onboard equipment can be identified. Using sensor signals, flight controller commands and possibly other data, an FDI algorithm detects faults in the actuators and sensors, e.g. stuck control surfaces or bias in the sensor measurement. An FDI solution is often part of a safety system that is capable of reconfiguring other components of the flight control system to compensate for the detected failure as described by [20].

A popular approach to FDI is to design optimal filters that estimate the difference between the actual control surface deflection and the control command, or the actual measured quantity and the sensor signal, calculating suitable residuals. (See [17]). An optimal H_∞ filter is designed by [8] to detect faults in the elevator actuator and pitch rate sensor for the Boeing 747. To use optimal filter design for FDI, an appropriate model of the aircraft is required. With the rise of flexible airframes even in commercial aviation, models that include flexible behaviour may be required for certain tasks. A flexible aircraft model is generally difficult to obtain as opposed to the classical rigid model which is usually the result of identification. The flexible model also requires more expertise to create, is generally more complex than the rigid one and it is subject to more uncertainty due to the substantial increase in model parameters. To compare the difficulties, see e.g. the construction of a flexible aircraft model by [24] and the classical rigid model by [16]. This part aims to give guidelines on what FDI performance requirements necessitate the use of a flexible aircraft model.

For the flexible aircraft of the FLiPASED project, we want to detect two faults in the longitudinal motion of the aircraft: angle of attack sensor and elevator actuator faults. (Note that the tail of the aircraft is outfitted with ruddervators, therefore it would be more precise to say that we want to detect a fault in the ruddervators that affect the longitudinal motion of the aircraft. We will continue to refer to the control surface as elevator for simplicity.) The block diagram of the FDI filter design problem is depicted in Figure 1. We design optimal FDI filters with different bandwidths using the rigid and the flexible model of the aircraft. Then, using a simple decision mechanism, we calculate the smallest detectable fault and the detection time for each fault and for each filter. Based on these results, we make recommendations on what sensor configuration and which model to use for certain performance requirements.

The rest of the chapter is structured as follows. In Subchapter 2.1, the flexible and the rigid model of the aircraft is outlined along with the sensors and actuators. Subchapter 2.2 describes how the optimal FDI filters are designed. The details of the performance evaluation of the filters (the calculation of the smallest detectable fault and detection time among others) is given in Subchapter 2.3. Subchapter 2.4 compares the achievable performance of the various filter designs and gives recommen-

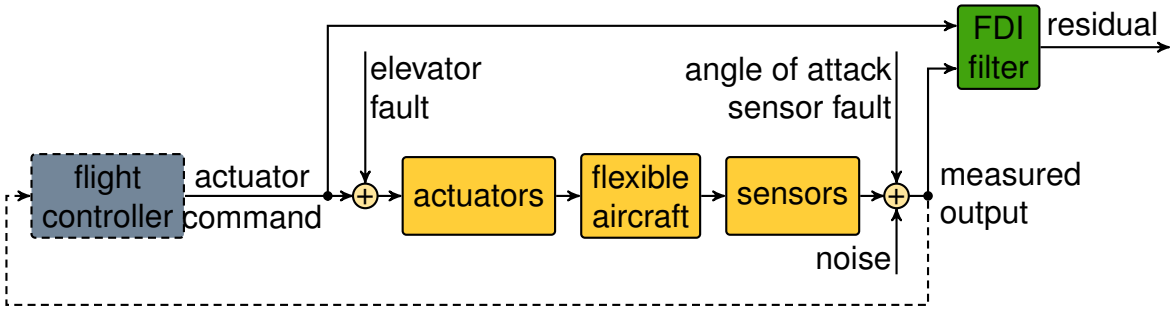

Figure 1: Block diagram of the joint actuator and sensor fault detection problem.

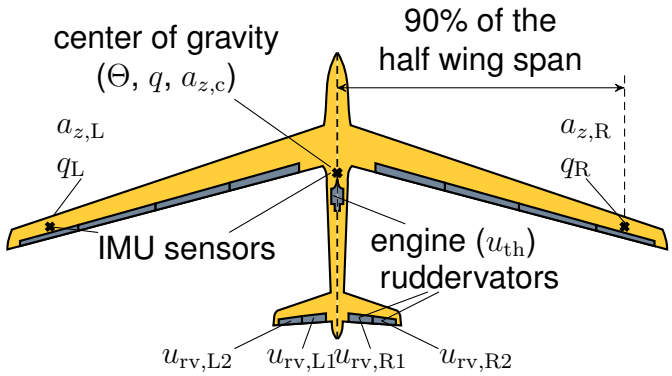

Figure 2: Control surface configuration and sensor positions of the flexible aircraft. The control inputs and sensor signals are marked at the corresponding control surfaces and sensors.

dations on when to use a flexible aircraft model. Finally, our findings are summarised in Subchapter 2.5.

2.1 The flexible and rigid aircraft model

The sensors and actuators relevant for the fault detection are illustrated in Figure 2. Two models of this aircraft are used for filter design in this chapter: a low order rigid body and a higher order flexible model. Both are linear longitudinal models obtained in straight and level flight (at $38\,\mathrm{m/s}$). A detailed description is given by [26] and [24].

The outputs are the sensor signals that consist of the angle of attack (α), pitch angle (Θ), pitch rate (q), speed (V), vertical acceleration in the centre of gravity ($a_{z,\mathrm{c}}$), and the mean of the acceleration and angular rate signals from the IMU's located close to the wing tips ($a_{z,\mathrm{w}} = (a_{z,\mathrm{L}} + a_{z,\mathrm{R}})/2$, $q_{\mathrm{w}} = (q_{\mathrm{L}} + q_{\mathrm{R}})/2$, the 'w' stands for 'wing'). The

Table 1: Sensor bandwidth and standard deviation of the measurement noise.

	$a_{z,\mathrm{c}}$	q	Θ
type	MTI-G-710 xSense		
bandwidth (θ)	$200\,\mathrm{Hz}$		
std. dev. of the noise	$0.08\,\mathrm{m/s^2}$	$0.3^\circ/\mathrm{s}$	$0.6^\circ/\mathrm{s}$
	V	α	
type	micro Air Data System 2.0		
bandwidth (θ)	$50\,\mathrm{Hz}$		
std. dev. of the noise	$0.33\,\mathrm{m/s}$	$0.33^\circ/\mathrm{s}$	
	$a_{z,\mathrm{w}}$	q_{w}	
type	MPU-9250		
bandwidth (θ)	$200\,\mathrm{Hz}$		
std. dev. of the noise	$0.72\,\mathrm{m/s^2}$	$5.4^\circ/s$	

sensors are modelled as first order low pass filters of the form

$$G_{\mathrm{sens}}(s) = \frac{1}{\frac{s}{2\pi\theta}+1}, \tag{1}$$

where θ is the bandwidth. Additive white noise is assumed on the sensor outputs. Based on the documentation of the sensors and experimental data, the standard deviations of the sensor noises along with the bandwidths are listed in Table 1.

The thrust command for the engine is denoted by u_{th}. The tail control surfaces are ruddervators with the commands $u_{\mathrm{rv,L1}}$, $u_{\mathrm{rv,L2}}$, $u_{\mathrm{rv,R1}}$, and $u_{\mathrm{rv,R1}}$ in Figure 2. These are used symmetrically, i.e. $u_{\mathrm{rv,L1}} = u_{\mathrm{rv,L2}}$ and $u_{\mathrm{rv,R1}} = u_{\mathrm{rv,R2}}$. The elevator command considered in this chapter is obtained by

$$u_{\mathrm{e}} = \frac{u_{\mathrm{rv,L1}} + u_{\mathrm{rv,R1}}}{2} = \frac{u_{\mathrm{rv,L2}} + u_{\mathrm{rv,R2}}}{2}. \tag{2}$$

Thus, the input of the system is the control command $u_{\mathrm{c}} = \begin{bmatrix} u_{\mathrm{e}} & u_{\mathrm{th}} \end{bmatrix}^T$. Based on experiments, the engine dynamics can be approximated by

$$G_{\mathrm{act,th}}(s) = \frac{1}{8s+1}. \tag{3}$$

The actuator dynamics for the elevator (for the ruddervators) is

$$G_{\mathrm{act,e}}(s) = \frac{1817}{s^2 + 54.03s + 1817}. \tag{4}$$

Since the ruddervators are transformed to a single elevator, only one actuator is included in the model. The input of the aerodynamics consists of the control surface

deflection, its derivative and second derivative, hence the derivatives of the output of $G_{\mathrm{act,e}}(s)$ are also connected to the system.

The state of the system consist of the velocity components along the longitudinal and vertical axis of the body frame (u and w respectively), pitch angle (Θ), pitch rate (q), five modal coordinates and their derivatives, two lag states, and three actuator states. The frequency of the short period mode and the first bending mode of the structural dynamics have special significance in the final analysis (in chapter 2.4). These are $\omega_{\mathrm{sp}} = 9\,\mathrm{rad/s}$ and $\omega_{\mathrm{fb}} = 18\,\mathrm{rad/s}$, respectively.

The rigid aircraft model is obtained by residualising the flexible states (modal coordinates, their derivatives, and the lag states). In practice, a rigid model is usually the result of parameter identification of a standard rigid model. Our approach aims to avoid any differences between the two models that do not arise from flexibility.

2.2 Fault detection filter design

The FDI filter design is articulated as an H_∞ optimal synthesis problem similarly to the solution of [8]. The generalised plant interconnection is depicted in Figure 3. Here, $f = \begin{bmatrix} f_{\mathrm{a}} & f_{\mathrm{s}} \end{bmatrix}^T$ is the fault which is modelled as an additive disturbance on the elevator actuator command and the angle of attack measurement. The output of the FDI filter $F(s)$ is called the residual. It is the estimate of the fault signal hence it is denoted by $\hat{f} = \begin{bmatrix} \hat{f}_{\mathrm{a}} & \hat{f}_{\mathrm{s}} \end{bmatrix}^T$. The control command u_{c} is normally the output of the flight controller but since no controller is considered in the design process, it is treated as a known external disturbance.

The desired response of the residual signals to the faults is defined as

$$T_{\mathrm{des}}(s) = \frac{1}{\kappa s + 1} I_2, \tag{5}$$

where I_2 is a 2×2 identity matrix. The time constant κ is a design parameter that sets the required bandwidth (hence the speed of the response). Noise cancellation is required on the frequency range beyond the bandwidth of $T_{\mathrm{des}}(s)$. This is captured by the noise weighting function

$$W_{\mathrm{n}}(s) = R \frac{10\sqrt{2}\kappa s + 1}{\frac{\sqrt{2}\kappa}{100} s + 1}, \tag{6}$$

where R is a diagonal matrix with the standard deviations of the individual noise signals in the diagonal. The weight of the estimation error is also chosen to correspond to the bandwidth of $T_{\mathrm{des}}(s)$. It is defined as

$$W_{\mathrm{e}}(s) = \frac{0.01\kappa s + 1}{\kappa s + 1} I_2. \tag{7}$$

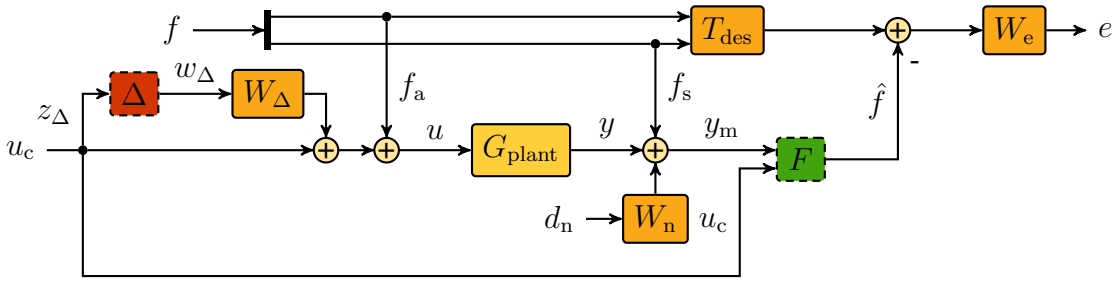

Figure 3: Generalized plant interconnection for the H_∞ FDI filter design.

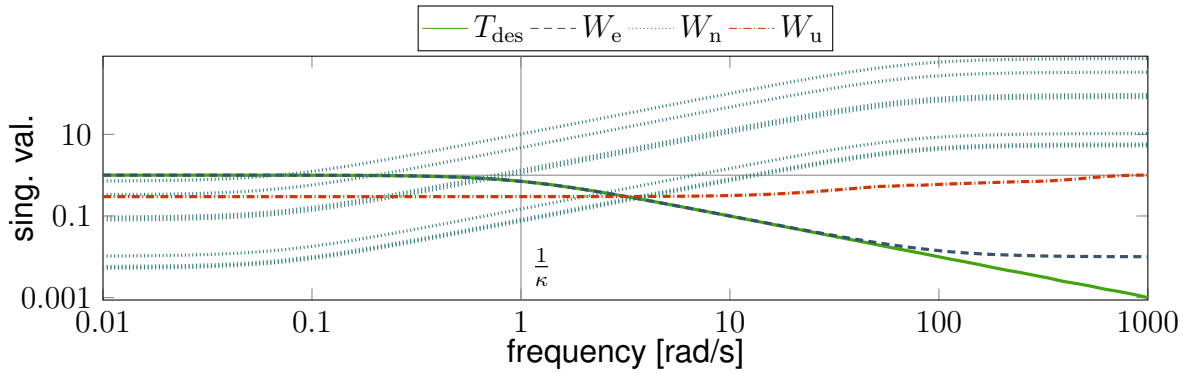

Figure 4: Weighting functions used for the H_∞ synthesis. The value of the design parameter is $\kappa = 1\text{s}$. (Since the standard deviations of the noise channels are different, $W_{\text{n}}(s)$ is represented by multiple lines.)

The weight of the input multiplicative uncertainty is

$$W_{\text{u}}(s) = \frac{(s + 24.71)\,(s^2 + 121.9s + 2 \cdot 10^4)}{(s + 64.24)\,(s^2 + 138.2s + 2.6 \cdot 16^4)}. \tag{8}$$

This is chosen so that the uncertain plant

$$G_{\text{plant}}(s)\,(I_2 + W_{\text{u}}(s)\,\Delta(s)) \tag{9}$$

has 30% uncertainty on low frequencies, 50% at the elevator actuator bandwidth, and 100% at high frequencies. Notice that $W_{\text{u}}(s)$ does not depend on κ since it describes the accuracy of the model regardless of the bandwidth requirement. These weighting functions for $\kappa = 1\text{s}$ are compared in Figure 4.

Denote the interconnected system depicted in Figure 3 with $F(s)$ and $\Delta(s)$ cut out by

$$\begin{bmatrix} z_\Delta \\ e \\ y_{\text{m}} \\ u_{\text{c}} \end{bmatrix} = M(s) \begin{bmatrix} w_\Delta \\ f \\ u_{\text{c}} \\ d_{\text{n}} \\ \hat{f} \end{bmatrix}. \tag{10}$$

To connect $\Delta(s)$ and $F(s)$, let us define the Linear Fractional Transformations (LFTs). For any two complex matrix (or dynamic system) $X = \begin{bmatrix} X_{11} & X_{12} \\ X_{21} & X_{22} \end{bmatrix}$ and Y, the upper LFT exists if X_{11} has the same size as Y^T and it is defined as

$$\mathcal{F}_U(X,\, Y) = X_{21}Y\left(I - X_{11}Y\right)^{-1} X_{12} + X_{22}. \tag{11}$$

Similarly, if X_{22} has the same size as Y^T, then

$$\mathcal{F}_L(X,\, Y) = X_{12}Y\left(I - X_{22}Y\right)^{-1} X_{21} + X_{11}. \tag{12}$$

The uncertain generalised plant is then

$$P(\Delta,\, s) = \mathcal{F}_U(M(s),\, \Delta(s))\,. \tag{13}$$

The objective of the design is to find a filter $F(s)$ such that the H_∞ norm of

$$\mathcal{F}_L(P(\Delta,\, s),\, F(s))$$

is minimal for all possible uncertainties, i.e the optimisation problem is

$$\min_{F(s)} \max_{||\Delta(s)||_\infty \leq 1} ||\mathcal{F}_L(P(\Delta,\, s),\, F(s))||_\infty\,. \tag{14}$$

Since $P(\Delta,\, s)$ is robustly stable (stable for all admissible $\Delta(s)$), this is equivalent to

$$\min_{F(s)} ||\mathcal{F}_L(M(s),\, F(s))||_\infty\,. \tag{15}$$

This optimization is solved using the standard H_∞ synthesis tool implemented in the `hinfsyn` function of MATLAB. For details about the robust design technique, see [11].

2.3 Evaluation of the fault detection performance

For the evaluation of the FDI filter, the weighting functions and performance output channels are removed from the generalized plant in Figure 3. Hence, we consider the interconnection in Figure 5. Here, $F(s)$ is the filter designed by the process described in Chapter 2.2. Let us denote the system in Figure 5 by

$$\hat{f} = T(\Delta,\, s) \begin{bmatrix} f \\ u_c \\ n \end{bmatrix} \tag{16}$$

For simplicity, we only describe the tools we use to evaluate the performance of the actuator fault detection. The calculations employed for the sensor fault detection evaluation are identical. The theoretical background of the computations involved in this chapter is described by [11].

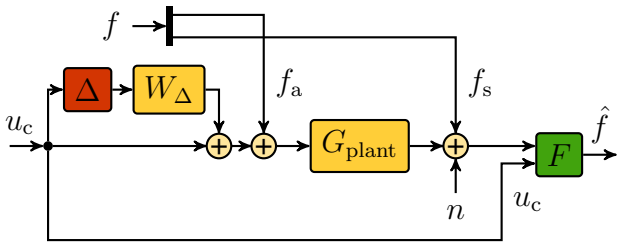

Figure 5: Interconnection of the uncertain aircraft model and the H_∞ FDI filter design used in the performance evaluation.

The effect of the control command on the residual is measured by the worst-case gain of $T(\Delta,\, s)$ from the input u_c to the output $\hat{f}_\mathrm{a}$. Denote this gain by

$$\vartheta_\mathrm{a} = \max_{||\Delta(s)||_\infty \leq 1} \left|\left| T_{\hat{f}_\mathrm{a} \leftarrow u_\mathrm{c}}(\Delta,\, s)\, \Lambda_u \right|\right|_\infty , \tag{17}$$

where $\Lambda_u = \mathrm{diag}(15^\circ,\, 0.2)$ is a scaling matrix that represents the maximum control input. We use the approximation that if there is no noise and fault in the system (i.e. $n = 0$ and $f = 0$), then the residual produced by the control command alone is at most ϑ_a (i.e. $\hat{f}_a \leq \vartheta_\mathrm{a}$) for all admissible values of the uncertainty $\Delta(s)$. Note that strictly speaking, instead of the H_∞ norm, the induced L_∞ should be used. However, the induced L_∞ norm is difficult to compute in the presence of uncertainty. Also, these two norms bound each other up to a constant factor, therefore trends we want to observe are not influenced by the choice of the norm.

The effect of the noise on the residual is captured by the standard deviation of $\hat{f}_\mathrm{a}$ due to the noise. This is calculated as the H_2 norm of $T(\Delta,\, s)$ from n to $\hat{f}_\mathrm{a}$, i.e.

$$\sigma_\mathrm{a}^2 = \left|\left| T_{\hat{f}_\mathrm{a} \leftarrow n}(0,\, s)\, R \right|\right|_2 . \tag{18}$$

Recall that R is a diagonal matrix with the standard deviations of the noise signals on the diagonal. We use $\Delta(s) = 0$ to indicate that the value of $\Delta(s)$ is arbitrary in this computation since our model assumes no uncertainty in the system in the channels from the noise to the residual.

The above quantities are used to define the detection time and the smallest robustly detectable fault. We use a simple threshold decision logic to decide whether a fault actually occurred. In the practical implementation of an FDI system, an integration-based or an up-down counter-based decision logic is usually used as described by [25], and [15] respectively. Our simple threshold logic approximates the behavior of those more complex solutions. The decision threshold is the maximum residual caused by the control input plus one standard deviation of the residual signal, i.e. $\vartheta_\mathrm{a} + \sigma_\mathrm{a}$.

If the residual is $\vartheta_\mathrm{a} + 1.3\sigma_\mathrm{a}$ in steady-state and without noise, then the probability that $\hat{f}_\mathrm{a} > \vartheta_\mathrm{a} + \sigma_\mathrm{a}$ in the presence of noise is 90%. Therefore, we call the fault corresponding

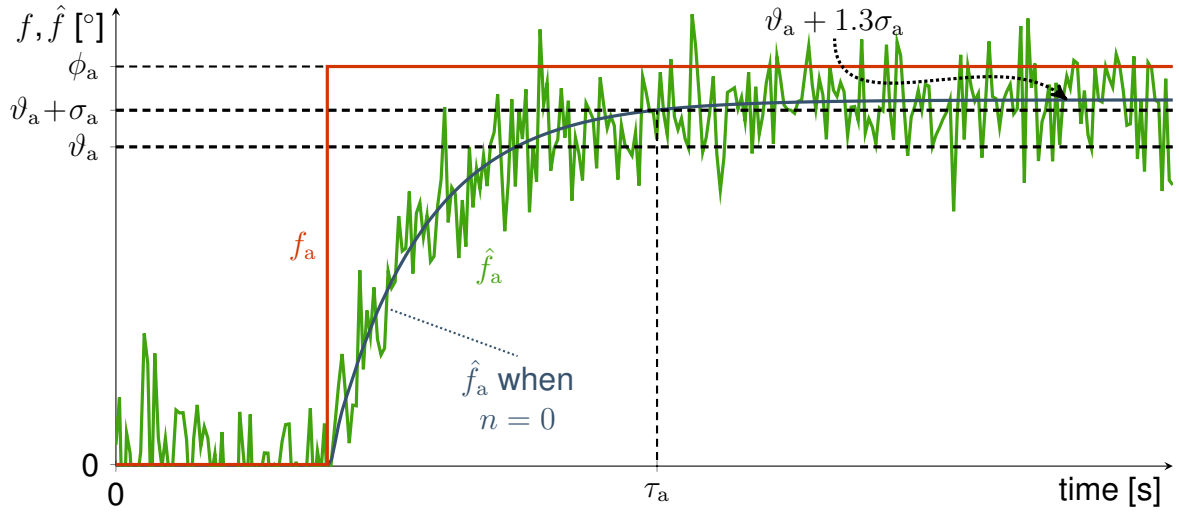

Figure 6: Definition of the detection time and smallest detectable fault.

to this residual the smallest robustly detectable fault. It is denoted by ϕ_a and is defined by the equation

$$T_{\hat{f}_a \leftarrow f_a}(0,\, 0)\, \phi_a = \vartheta_a + 1.3\sigma_a. \tag{19}$$

Note that similarly to the noise, there is no uncertainty in the channels from f to $\hat{f}$. Therefore, the uncertainty sample $\Delta(s) = 0$ is used again in the computations. In accordance with the definition of ϕ_a, the detection time τ_a is defined as the time when the step response of $T_{\hat{f}_a \leftarrow f_a}(0,\, s)\, \phi_a$ crosses the threshold $\vartheta_a + \sigma_a$. These quantities are illustrated in Figure 6.

To contrast the results with frequency domain data, we also define the bandwidth of the FDI filter $F(s)$. We define the bandwidth as the frequency above which the singular value of the filter to the $\hat{f}_a$ output channel is less than $-6\,\mathrm{dB}$. I.e. B_a is the bandwidth of $F_{\hat{f}_a}(s)$ if $\bar{\sigma}(F_{\hat{f}_a}(j\omega)) < -6\,\mathrm{dB}$ for $\omega > B_a$. This definition means that almost all of the frequency content of $\hat{f}_a$ is concentrated in the frequency interval $[0,\, B_a]$.

Finally, we demonstrate these analysis metrics by evaluating the filter design for $\kappa = 0.5\,\mathrm{s}$ and $\kappa = 0.2\,\mathrm{s}$. For this filter design, we use the measurements α, Θ, q, V, and $a_{z,c}$. (A detailed evaluation for multiple values of κ and different sensor configurations is presented in Chapter 2.4.)

When $\kappa = 0.5\mathrm{s}$, the resulting filter bandwidths are $B_a = 3.11\,\mathrm{rad/s}$ and $B_s = 3.41\,\mathrm{rad/s}$. At these frequencies, the model uncertainty is still low, therefore design conditions can be met. The effect of the control input to the residuals is $\vartheta_a = 4.08°$ and $\vartheta_s = 0.06°$. Since f_a acts on the input of the system and the input dynamics are uncertain, ϑ_a is much greater than ϑ_s. The noise on the other hand affects the estimation of f_s more. This is reflected by the values $\sigma_a = 2.62°$ and $\sigma_s = 4.35°$. The smallest detectable faults

and detection times are $\phi_{\mathrm{a}} = 8.16°$, $\phi_{\mathrm{s}} = 5.67°$, $\tau_{\mathrm{a}} = 1.16\,\mathrm{s}$, and $\tau_{\mathrm{s}} = 0.78\,\mathrm{s}$. According to both performance measures, the sensor fault detection problem proves easier to solve. If we conduct this analysis using the filter designed for the rigid model, we get $\phi_{\mathrm{a}} = 8.21°$, $\phi_{\mathrm{s}} = 5.90°$, $\tau_{\mathrm{a}} = 1.17\,\mathrm{s}$, and $\tau_{\mathrm{s}} = 0.81\,\mathrm{s}$. These values are very close to the previous ones therefore we can conclude that if this performance is satisfactory to our goals, it is sufficient to carry out the filter design using the rigid model.

If $\kappa = 0.2\,\mathrm{s}$ however, the difference is greater for the actuator fault estimation. In this case, the bandwidths are higher: $B_{\mathrm{a}} = 7.96\,\mathrm{rad/s}$ and $B_{\mathrm{s}} = 8.54\,\mathrm{rad/s}$. This causes the detection time to decrease to $\tau_{\mathrm{a}} = 0.41\,\mathrm{s}$ and $\tau_{\mathrm{s}} = 0.31\,\mathrm{s}$. This is achieved at the cost of lower sensitivity to the faults which is expressed by the increase in the smallest detectable faults: $\phi_{\mathrm{a}} = 11.16°$ and $\phi_{\mathrm{s}} = 7.08°$. When the filter is designed for the rigid model, these values become $\tau_{\mathrm{a}} = 0.55\,\mathrm{s}$, $\tau_{\mathrm{s}} = 0.32\,\mathrm{s}$, $\phi_{\mathrm{a}} = 13.57°$ $\phi_{\mathrm{s}} = 7.59°$. At this bandwidth, the rigid and flexible models are more different than in the previous case (for $\kappa = 0.5\,\mathrm{s}$) therefore the difference between the performance measures are more pronounced. The degradation is especially significant for the actuator fault estimation.

2.4 Comparison of the rigid and flexible model based designs

In this chapter, we compare the FDI filters designed for the rigid and flexible aircraft models. The performance metrics we consider are the detection time, smallest detectable fault and filter bandwidth as defined in Chapter 2.3. In order to study the usefulness of acceleration measurements (and q_{w}), three sensor configurations are compared:

no acc.:	α, Θ, q, V
acc.:	α, Θ, q, V, $a_{z,\mathrm{c}}$
acc. +w:	α, Θ, q, V, $a_{z,\mathrm{c}}$, $a_{z,\mathrm{w}}$, q_{w}.

Our calculations revealed that the accelerometers placed close to the wing tips do not improve FDI performance since there is no difference in performance between the configurations labelled 'acc.' and 'acc. +w'. Hence, we only compare configuration 'no acc.' and 'acc.' in the rest of this chapter. Figs. 7-12 present the data that are the basis of the comparison. Each figure has graphs that correspond to the flexible and rigid model-based designs (flex. and rigid) and to sensor configuration 'no acc.' and 'acc'.

Figure 7 presents the trade-off between the smallest detectable fault and the detection time for the actuator fault detection. If accelerometer measurements are used, the performance of the filters designed for the rigid and flexible models are very similar for $\tau_{\mathrm{a}} \geq 0.8\,\mathrm{s}$. If we aim to achieve lower detection time than $0.8\,\mathrm{s}$, then a flexible model is clearly required, since the performance curves diverge in this domain. In terms of

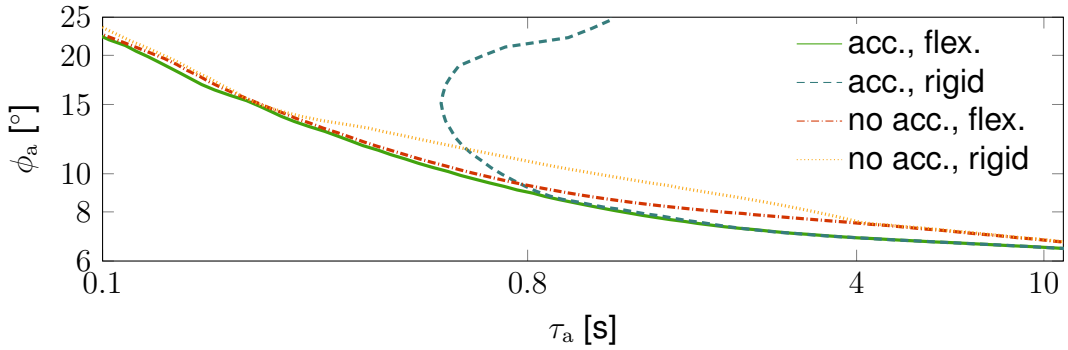

Figure 7: Trade-off between the smallest detectable fault and the detection time for the actuator fault detection.

filter bandwidth, this divergence is observable above half of the frequency of the short period mode ($\omega_{sp}/2$) in Figs. 8 and 9.

Without accelerometer measurements, the achievable performance is strictly worst but it is not affected by the choice of design model so heavily. There is noticeable difference between the two 'no acc.' curves in Figure 7 but the difference is less pronounced. As demonstrated by Figure 8, there is only a couple of degrees difference between the smallest detectable fault in the two cases. However, this difference persists on the entire bandwidth range of interest. On the other hand, the detection times are very close as illustrated in Figure 9. The ϕ_a and τ_a values are only plotted up to around $14\,\mathrm{rad/s}$ (close to ω_{fb}) because further improvement in the performance requires more than $60\,\mathrm{rad/s}$ filter bandwidth. (The corresponding data points are still shown in Figure 7, however.) This discontinuity occurs, because the lack of $a_{z,c}$ measurement hides the high frequency behaviour of the aircraft which results in a local peak in the filter gain that tends towards high frequencies. This local peak becomes prominent (greater than $-6\,\mathrm{dB}$) at around $60\,\mathrm{rad/s}$, causing the filter bandwidth to jump above $60\,\mathrm{rad/s}$.

The angle of attack sensor fault estimation is not affected as much by the model uncertainty and flexibility as the elevator actuator fault. Hence, faster and more precise fault detection is attainable overall. For low filter bandwidths (high detection times), the ϕ_s and τ_s values are very close for all four options in Figs 10-12. Similarly to the elevator fault detection, the difference between flexible and rigid model-based designs only show if we aim for low detection times. The difference however, is small (less than one degree) for the domain of our analysis. The worst performance clearly corresponds to the case when no acceleration measurement is used and the filter is designed for the rigid model. But since the performance measures track close to each other for all four cases, we conclude that the performance of the angle of attack sensor fault detection is not impacted greatly by the choice of design model or sensor configuration.

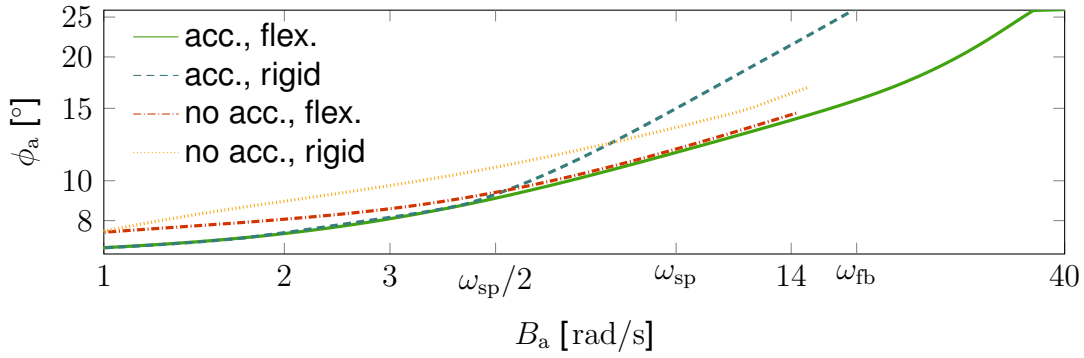

Figure 8: Comparison of the smallest detectable actuator faults as a function of filter bandwidth.

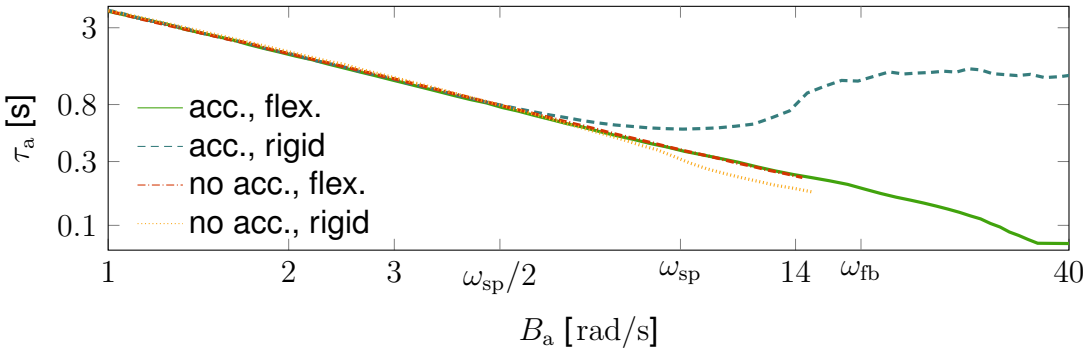

Figure 9: Comparison of the detection times of the actuator fault detection as a function of filter bandwidth.

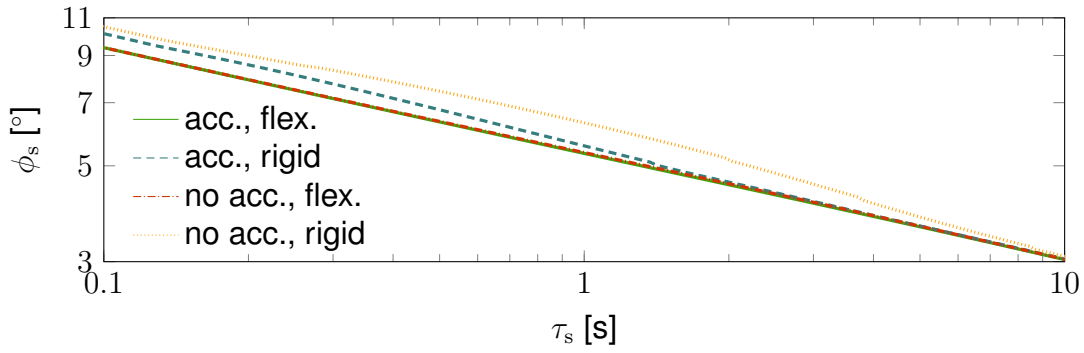

Figure 10: Trade-off between the smallest detectable fault and the detection time for the sensor fault detection.

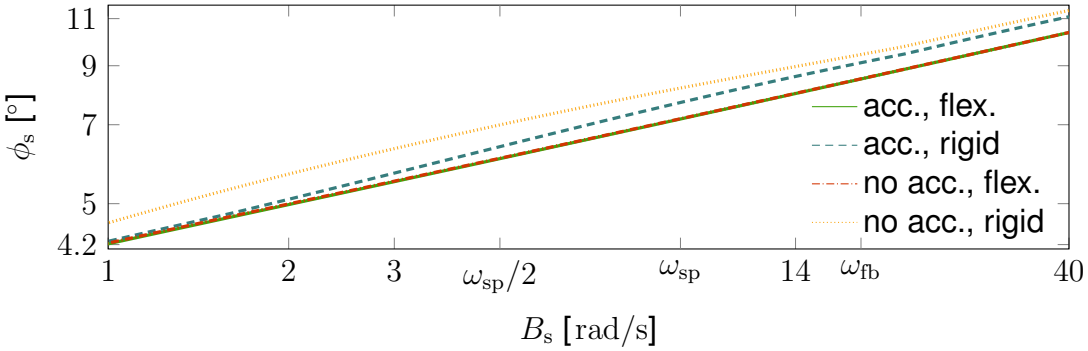

Figure 11: Comparison of the smallest detectable sensor faults as a function of filter bandwidth.

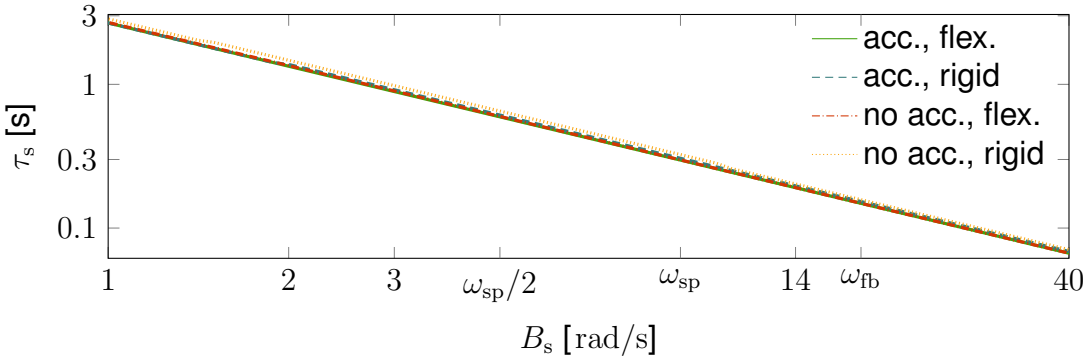

Figure 12: Comparison of the detection times of the sensor fault detection as a function of filter bandwidth.

2.5 Summary of the recommendations

Using a specific case study, guidelines are established on when a flexible model is required for FDI filter design for a flexible aircraft. It is concluded that only minor performance improvement is attainable for the angle of attack sensor FDI with the involvement of the flexible model. In contrast, the elevator FDI is greatly impacted by the choice of sensor configuration and design model. If good performance is expected at high frequencies (beyond the frequency of the first bending mode), then both acceleration measurement at the center of gravity and the flexible model are required. Still using the acceleration measurement, good performance is achieved using the rigid model up to half of the frequency of the short period mode. At the cost of some loss in accuracy, a design based on the rigid model is capable of providing acceptable performance up the frequency of the first bending mode if the acceleration measurement is not used.

3 Synthesis of a Multiple-Model Adaptive Gust Load Alleviation Controller

For the synthesis of a Gust load alleviation controller aeroelastic models are needed. Often these models are linearized state-space systems defined at specific operating points within the flight envelope [18, 21, 28]. Adaptive control techniques provide the opportunity to adapt the flight controller to the prevailing conditions during the aircraft's operation and ensure optimal performance over a large range of operational conditions [14]. The simplest form of an adaptive controller is gain-scheduling, where a change in parameters, e.g. airspeed, is measured and used to adapt the controller by means of interpolation techniques within a grid of controllers [14]. There exists quite a rich literature on gain-scheduling techniques applied to flight control problems [6, 30, 22]. It is essential that the parameter used for gain-scheduling is directly measurable. However, there also exist variations in the system dynamics due to parameters, which cannot be easily measured. An important example is the mass distribution, which changes during the mission as the fuel level decreases. Especially, when tanks are located in the wings, a variation of the flexible mode shapes is the consequence [12]. Furthermore, it can be thought of uncertainties due to unmodelled dynamics or non-linearities in aerodynamic parameters, mass, damping and stiffness matrices and many more. In any of the mentioned cases it is necessary to somehow estimate the system behaviour. Indirect adaptive control offers the opportunity to estimate the current plant parameters with respect to the onboard measurements. Changes in the identified parameters then lead to an update of the controller gains. For the estimation of the plant parameters, however, it is difficult to guarantee that the excitation of the system is rich enough in its spectrum and that the parameters will eventually converge [14]. Direct adaptive control uses a single reference model providing the desired system outcomes. The difference with the real system measurements yields a residual used for control gain update [14]. A major limitation of this approach is its sensitivity to process and sensor noise in the presence of unmodelled dynamics [2]. Due to the limitations of the discussed approaches, within FliPASED multiple-model adaptive control (MMAC) is further analysed. The idea is to identify the model, among a predefined set of models, that describes the plant behaviour best and switch to the corresponding controller. Generally, there exist several scientific studies on the MMAC, see, e.g., [4, 5, 10, 14, 12]. [12] proposes model detection filters based on fault detection techniques to identify the best fitting model. Within FliPASED the method of [12] is applied to the demonstrator aircraft for a GLA controller. To cover different mass cases, at first, masses are artificially attached in a dedicated modelling process to the structural wing model in order to generate a significant variation in the flexible modes. For each mass case a GLA controller is synthesized and a switching logic is designed, that selects the most suitable controller based on the aircraft's current mass condition.

3.1 Control-Oriented Modelling

The aeroservoelastic modelling process comprising the structural and aerodynamic model is described in detail in [13, 29]. The gust is modelled as a vertical 1-cos gust, like shown in Figure 13. The gust velocity is given by U_{gust} and the gust half

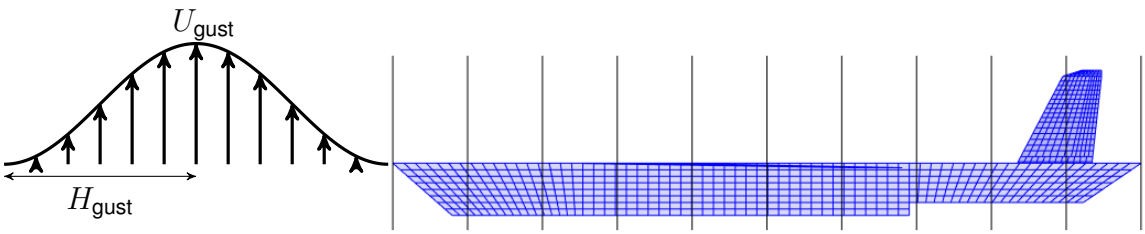

Figure 13: 1-cos gust and aircraft gust zones

length by H_{gust}. With increasing time the gust moves to the aft of the aircraft. In each gust zone, which are depicted as the regions between two vertical lines of the panel model in Figure 13, the corresponding aerodynamic panels are affected by the gust speed, that is observed at the front edge of the gust zone. Namely, within a gust zone the gust speed is constant. Instead of calculating the gust speed for each individual aerodynamic panel, this approach is an approximation, which saves a lot of computation time and is accurate enough for the considered application [7]. The difference of gust speeds in two neighbouring gust zones is defined by a time delay. As a transfer function a time delay can be defined by

$$G_{\text{delay}}(s) = e^{-t_{\text{delay}}s}, \tag{20}$$

where t_{delay} is the time delay in seconds and s is the Laplace variable [7]. To simplify the handling of time delays, it is approximated by a second order Padé approximation [19]

$$G_{\text{delay}}(s) \approx \frac{s^2 - \frac{6}{t_{\text{delay}}}s + \frac{12}{t_{\text{delay}}^2}}{s^2 + \frac{6}{t_{\text{delay}}}s + \frac{12}{t_{\text{delay}}^2}}. \tag{21}$$

Finally, the aircraft model can be described by

$$\begin{aligned} \dot{x} &= f(x, u, d) \\ y &= g(x, u) \end{aligned} \tag{22}$$

as a state-space model, where the states, inputs, disturbance and outputs are x, u, d and y. The inputs u comprise the commanded deflections to the control surfaces and the throttle command. The disturbance d provides an input of atmospheric turbulence, like a 1-cos gust, to the model. The outputs y summarize the onboard measurements and performance measurements, which here is the wing root bending moment

(WRBM). The WRBM is not measured, but is necessary for the GLA control synthesis. Equation (22) describes a non-linear state-space model. For the synthesis of a set of GLA controllers it is linearized leading to a set of linear time invariant (LTI) models.

3.2 MMAC GLA Synthesis

The goal of the GLA controller is to reduce the WRBM due to a vertical gust encounter. This should even be possible when the behaviour of the aircraft changes due to variations in the wing mass distribution. Masses are artificially attached to the structural model and the aeroelastic open-loop model is linearized for different mass cases. Furthermore, an appropriate GLA controller is synthesized per mass case. For each linearized model a residiuum generator is designed, in order to estimate which model describes the current aircraft behaviour best. Subsequently, the corresponding GLA controller is selected.

In the following the GLA synthesis procedure is provided for the standard mass case. It is the same for all mass cases. The selected measurements, which are fed into the controller, are the pitch angle θ, the pitch rate q_{fu} and the vertical accelerations measured in the fuselage $a_{z,\text{fu}}$ and on both wing tips $a_{z,\text{wl}}$ and $a_{z,\text{wr}}$. The control surfaces reacting to the gust encounter are the most outer ailerons on both wings and all four ruddervators of the tail, as shown in Figure 14. Thus the controller generates one

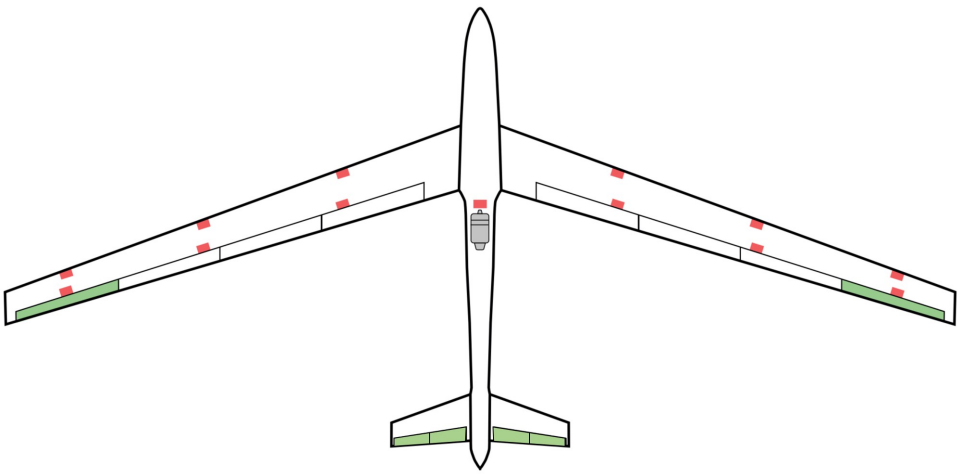

Figure 14: Demonstrator aircraft IMU (red) and control surface configuration [27]

signal u_{ail} connected to the ailerons and one signal u_{elev} connected to all four ruddervators. This simplification of signals is valid, as the aircraft is nearly symmetric and only vertical gust encounters are considered. Neglecting inputs and outputs unnecessary for the aircraft control the synthesis model reduces the number of states of Equation

(22) significantly. However, it still exhibits too many states, when it comes to an efficient GLA control synthesis. Therefore, the balanced reduction is used to decrease the order of the model even further [3].
The controller is synthesized with the structured $\mathcal{H}_\infty$ method [9]. It solves the optimisation problem

$$\underset{K\in\mathcal{K}}{min}||T_{d\to z}(K)||_\infty, \tag{23}$$

for which the $\mathcal{H}_\infty$ norm of the closed-loop weighted transfer function $T_{d\to z}(K)$ from a disturbance input d to a performance output z is minimized, while the structure of the controller K is predefined. Weighing the transfer function helps to limit the controller action to certain frequencies. Here the goal is to minimise the $\mathcal{H}_\infty$ norm of the transfer function from a 1-cos gust input d_{gust} to the weighted WRBM z_{wrbm} above $2\,\text{rad/s}$. Thus, it can be guaranteed that there is no interaction with the low frequency flight mechanics. Furthermore, the effort of the actuators z_{ail} and z_{elev} is limited as they feature rate and deflection limits. The control problem is outlined in form of a linear fractional transformation (LFT) representation as given in Figure 15. As a first step the controller is

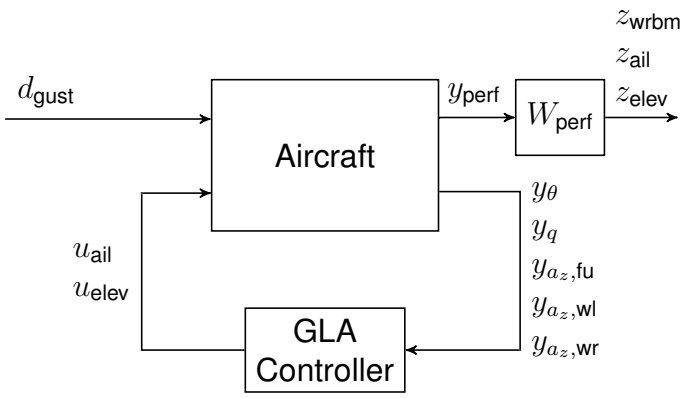

Figure 15: GLA controller

considered to be a 2×5 gain matrix. Hence 10 parameters have to be found. Figures 16 - 18 show the defined requirements (black), the open-loop (green) and closed-loop (blue) transfer functions for the structured $\mathcal{H}_\infty$ synthesis. It is visible from Figure 17 and Figure 18, that the deflection of the ailerons and the elevators stays within the predefined bounds, while the WRBM shown in Figure 16 can be generally reduced with a GLA controller in a frequency range of around $2-11\,\text{rad/s}$. The maximum peak of the open-loop WRBM at $58.4\,\text{rad/s}$ is reduced significantly. At various frequencies the closed-loop WRBM might exceed the one of the open-loop case, but an overall improvement is clearly visible. Time simulations of different gust excitations verify, that the maximum peak loads are decreased. Figure 19 shows the WRBM to a step excitation at the gust input d_{gust}. With the GLA controller a reduction of the maximum load of almost $10\,\%$ is achieved. In addition, two excitations refering to a 1-cos gust with frequency 58.4 and $25.6\,\text{rad/s}$ are considered. At $58.4\,\text{rad/s}$ Figure 16 shows a maximum raise in the WRBM for the open-loop system in the frequency domain. It can only

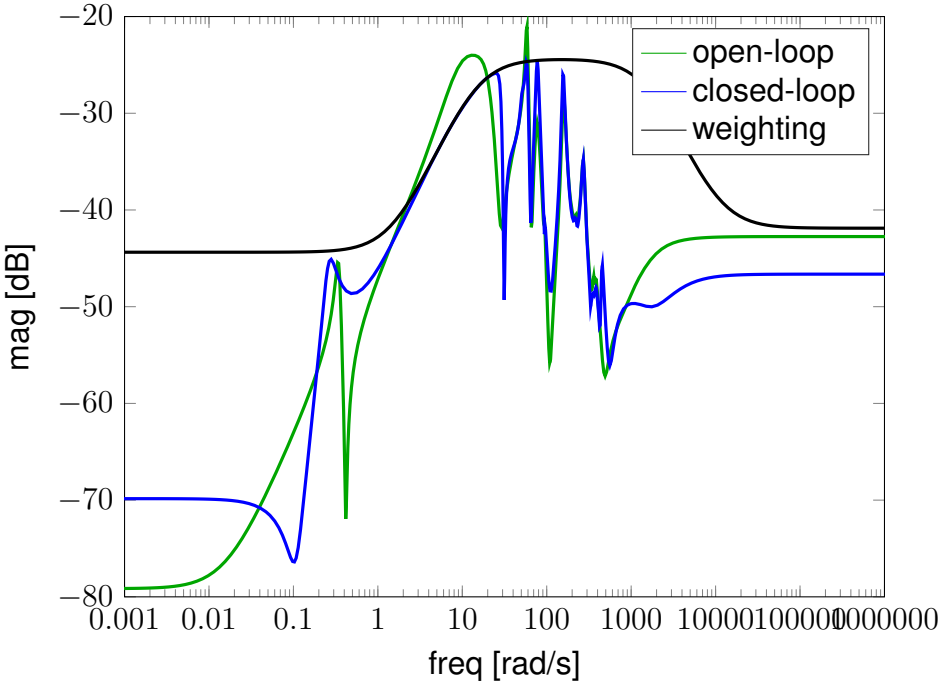

Figure 16: Wing root bending moment

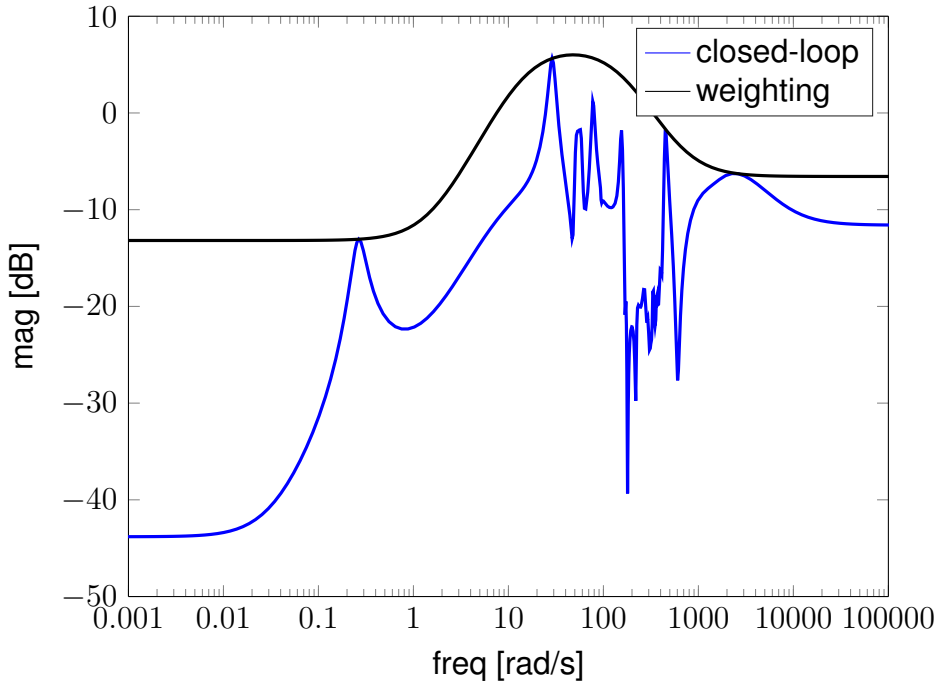

Figure 17: Requirement for outer ailerons

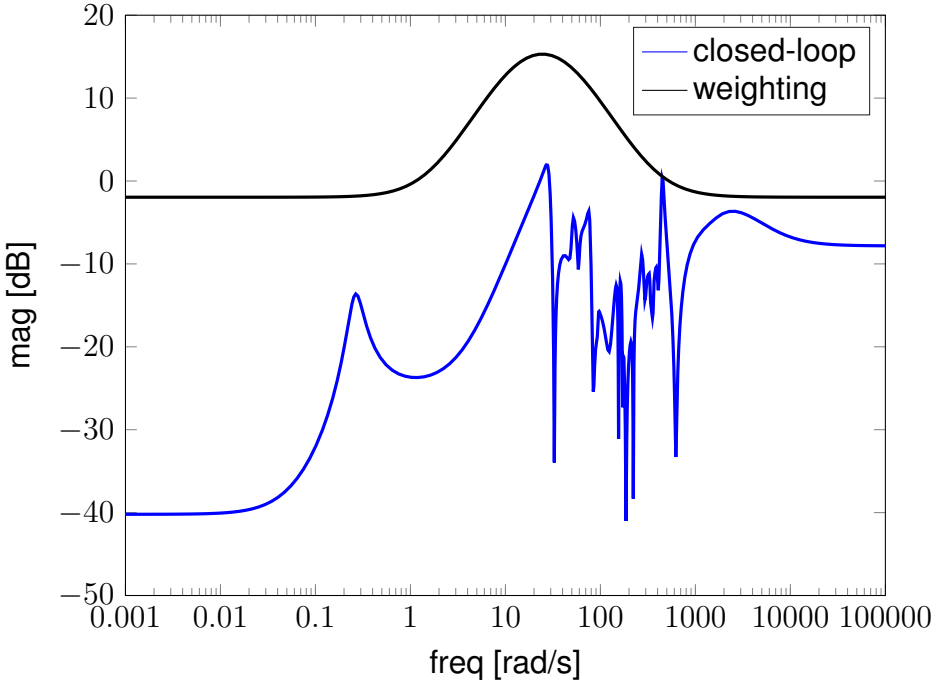

Figure 18: Requirement for elevators

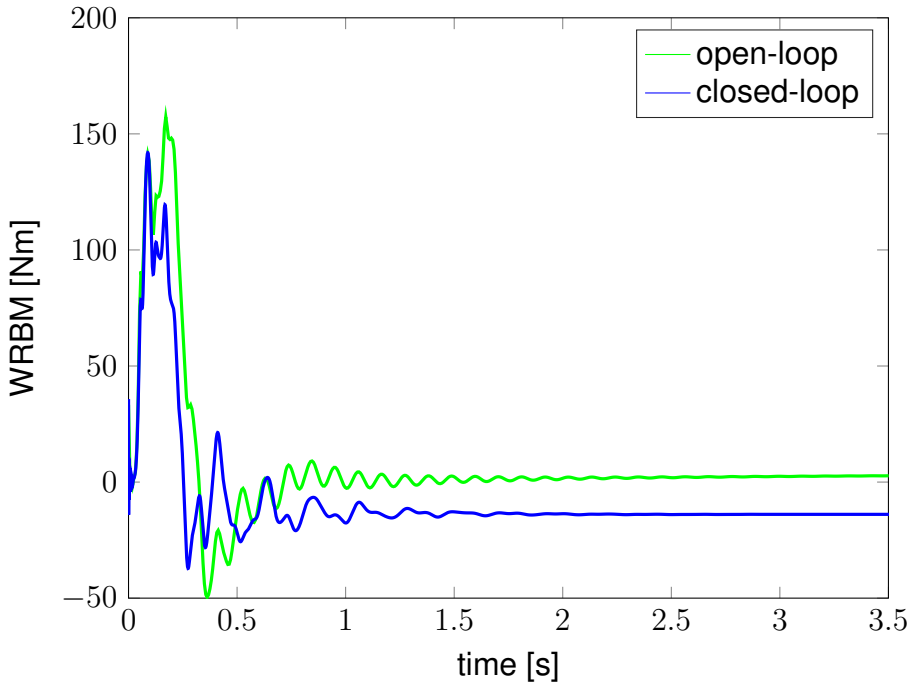

Figure 19: Step response to gust disturbance

be reduced by $3\,\%$ as shown in Figure 20. As the excitation by a discrete 1-cos gust

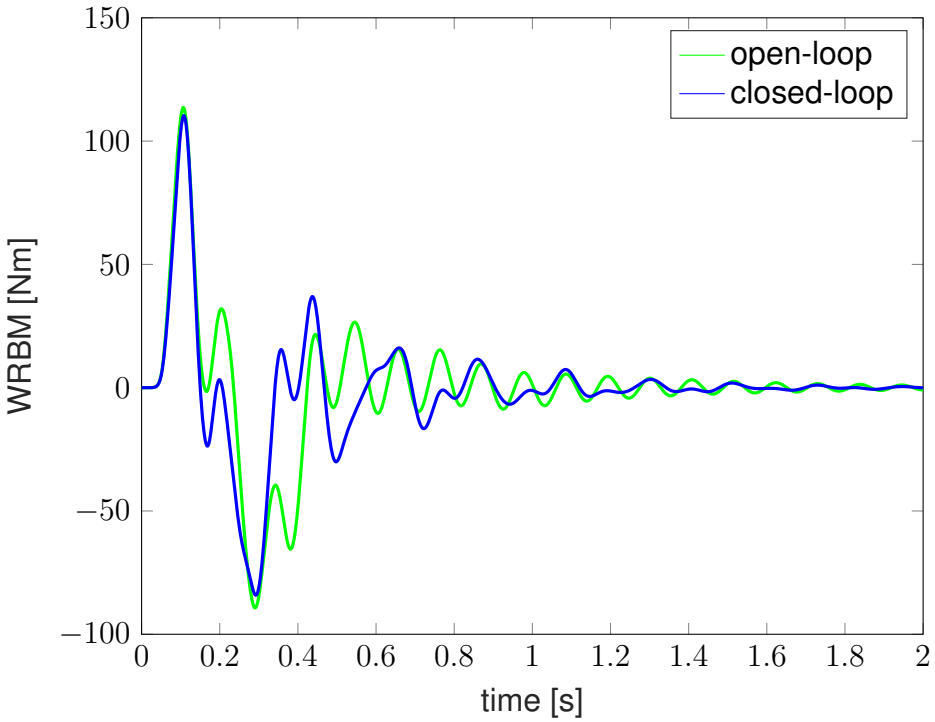

Figure 20: Response to 1-cos gust ($58.4\,$Hz)

cannot be restricted to a single frequency, but to a frequency band, the load reduction is not as high as expected. For the critical gust half length

$$H_{\text{gust,crit}} = 12.5 c_r \tag{24}$$

defined by Pratt, a nominal 1-cos gust excitation of $25.6\,\text{rad/s}$ is achieved [1]. The time simulation is shown in Figure 21. The maximum WRBM is reduced by almost $12\,\%$. However, the wing tends to vibrate longer.
For all aircraft mass cases a GLA controller is synthesized with the procedure stated above. Within the upcoming sections, it is assumed, that the grid of GLA controllers refering to different mass cases is available.

For the MMAC the identification of the best matching model is essential. From a set of N models, each defined at a different operating point, it is decided which model j represents the current plant behaviour best. It is assumed that the dynamics of the set of models ($j = 1, ..., N$) is given by the multiple LTI plant model

$$y_j(s) = G_j(s)u(s) + G_{d,j}(s)d(s), \tag{25}$$

where s is the Laplace variable, $y_j(s)$ represents the Laplace transformed output vector, $u(s)$ the Laplace transformed input vector, $d(s)$ the Laplace transformed distur-

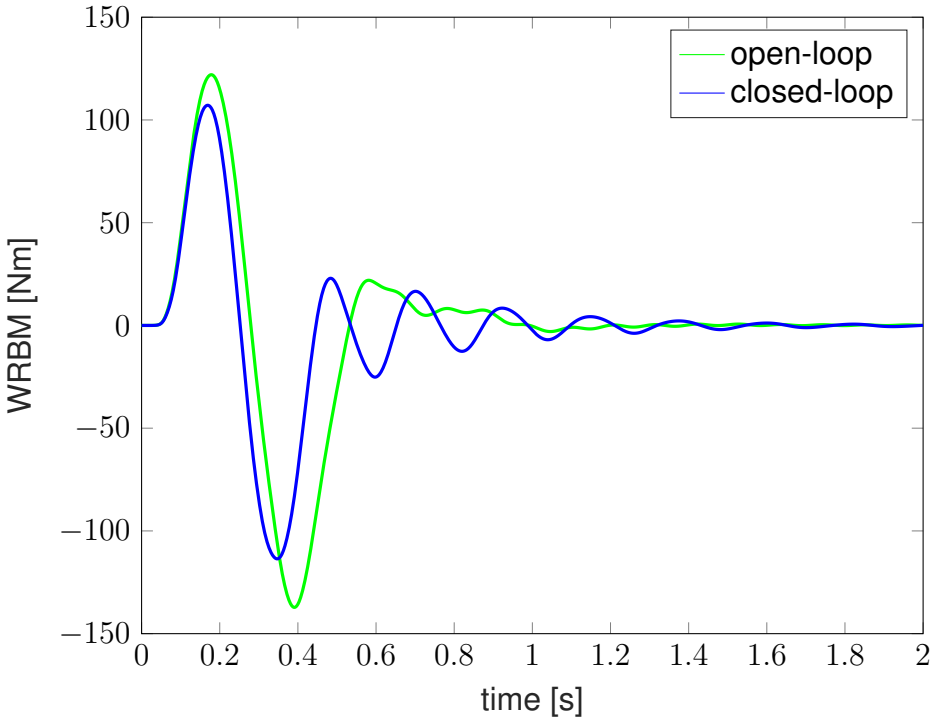

Figure 21: Response to 1-cos gust (25.6 Hz)

bance vector and $G_j(s)$ and $G_{d,j}(s)$ represent the control input to output and the disturbance input to output transfer function matrices, respectively [23].
The basic idea of model detection is depcited in Figure 22. The aircraft is affected by disturbance d and a varying parameter $p(t)$. The inputs u and outputs y of the plant are provided to the model detection system. For each model i a residual generation filter is defined, which then determines a residual r_i. The residual evaluator usually analyses r_i on the basis of a norm. This leads to the evaluation variable θ_i. The decision which model is judged to be the most valid one is taken by the lowest evaluated residual. In words, the lowest evaluated residual simply indicates the model with the lowest distance of all models to the currently active one.
The required residual filters $Q_i(s)$ relate the actual system inputs u and outputs y to the residuals $r_i(s)$ based on the ith system model. It therefore holds

$$r_i(s) = Q_i(s) \begin{bmatrix} y_j(s) \\ u(s) \end{bmatrix}, \; i = 1, ..., N, \tag{26}$$

where $r_i(s)$ is the Laplace transformed residual of the ith model detection filter $Q_i(s)$. Note that Equation (26) is the internal form of the ith filter driven by the jth model from the multiple plant model in Equation (25). Inserting the set of models from Equation (25) into the set of residual filters, Equation (26) leads to the internal form of the filter,

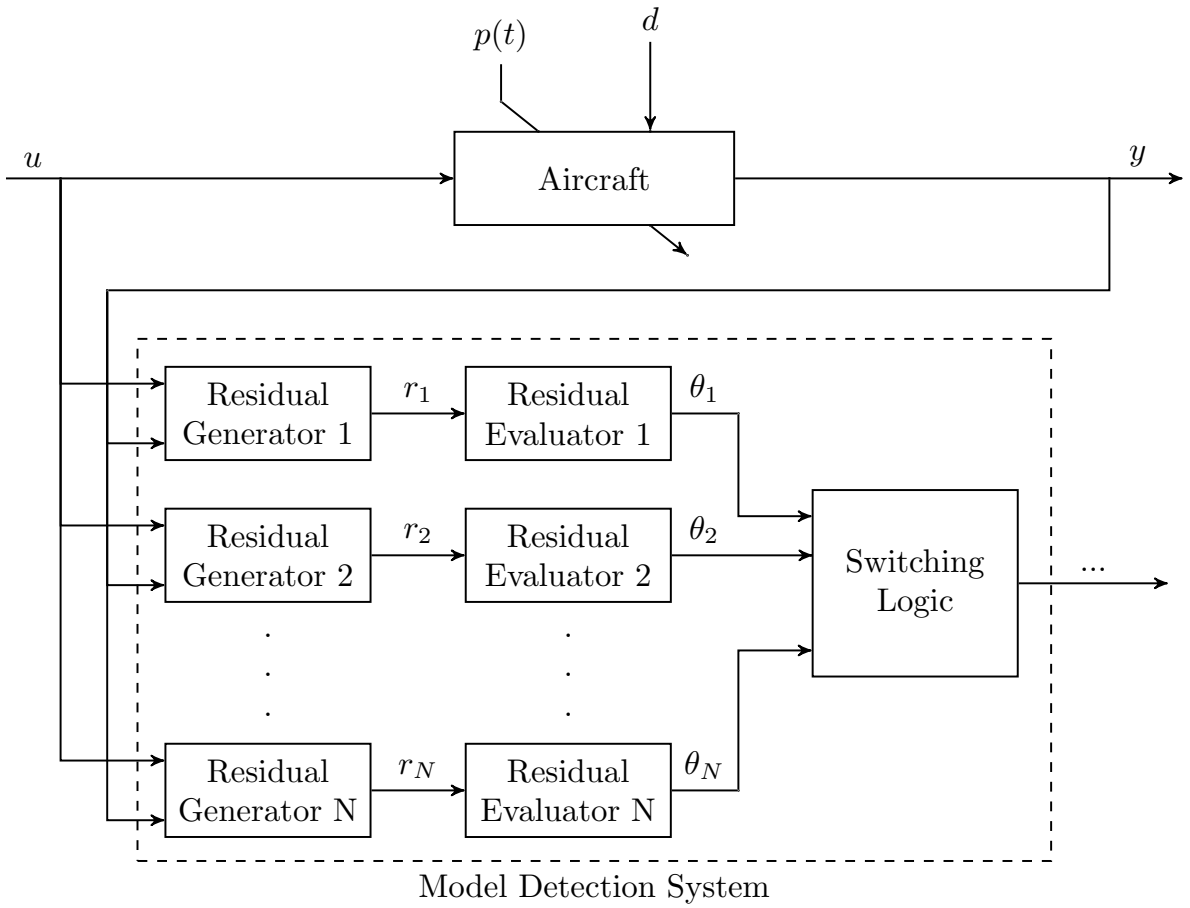

Figure 22: Model detection [23]

i.e.,

$$\tilde{r}_{ij}(s) = R_{ij}(s) \begin{bmatrix} u(s) \\ d(s) \end{bmatrix} = Q_i(s) \begin{bmatrix} G_j(s) & G_j(s) \\ I_u & 0 \end{bmatrix} \begin{bmatrix} u(s) \\ d(s) \end{bmatrix}. \tag{27}$$

The matrix I_u represents a unity matrix of the size of u [23].
Based on this internal filter form the model detection problem can be defined as follows:
For the multiple LTI system

$$y_j(s) = G_j(s)u(s) + G_{d,j}(s)d(s),\ j = 1, ..., N, \tag{28}$$

determine N stable filters $Q_i(s),\ i = 1, ..., N$, such that

$$(i)\ [R_{u,ii}(s)\ R_{d,ii}(s)] = 0,\ i = 1, ..., N,$$
$$(ii)\ R_{u,ij}(s) \neq 0,\ \forall j \neq i, \text{ and } [R_{u,ij}(s) R_{d,ij}(s)] \text{ stable.}$$

The solvability conditions of this problem can be found in [23]. Also, [23] presents adequate numerical tools to solve the problem.

3.3 Conclusion on MMAC for GLA

Changes in the mass properties of an aircraft during a mission due to e.g. defueling, can significantly affect the aeroelastic behaviour. Secondary control functions, like active GLA, MLA or active flutter suppression either have to be robust or have to be adapted to changing conditions. Adaption allows to increase the performance of control functions. MMAC offers a possibility to switch between a set of controllers designed at various operating points depending on the aircraft's state. Model detection algorithms can be used in order to select the "best" controller.
The development of a GLA controller based on MMAC is in progress in the FLiPASED project to explore such possibilities for flexible aircraft with changing mass.

4 Conclusion

In the deliverable first, the effect of structural flexibility on actuator and sensor fault detection filter design for the FLiPASED aircraft was explored by SZTAKI, second the possibility to develop a multiple model adaptive gust load alleviation controller considering the change of mass for the same aircraft was considered by DLR.

Finally, guidelines are established on when a flexible model is required for FDI filter design for the FLiPASED aircraft. It is concluded that only minor performance improvement is attainable for the angle of attack sensor FDI with the involvement of the flexible model. In contrast, the elevator FDI is greatly impacted by the choice of sensor configuration and design model. If good performance is expected at high frequencies (beyond the frequency of the first bending mode), then both acceleration measurement at the center of gravity and the flexible model are required. These guidelines will be considered by the consortium for future evaluation regarding other flexible aircraft and global FDI design guidelines for flexible wing structures will be presented if possible.

A MMAC structure offers the opportunity to control a complex system considering multiple working points. In case of the FLiPASED aircraft gust load alleviation controller design via MMAC approach is initiated considering the changes of aircraft mass in case of a flexible structure. The experiences with this design methodology will be utilized in the tightly coupled multi objective optimization aircraft design toolchain as generation of LTI models around system working points is straightforward and so gust load alleviation (and other) control can also be considered in design time leading to a more optimized aircraft-sensor-actuator-control structure.

5 Bibliography

[1] Kermit G. Pratt. “A Revised Formula for the Calculation of Gust Loads”. In: (1953).

[2] C. Rohrs et al. “Robustness of continuous-time adaptive control algorithms in the presence of unmodeled dynamics”. In: *IEEE Transactions on Automatic Control* 30.9 (1985), pp. 881–889. ISSN: 00189286. DOI: 10.1109/TAC.1985.1104070.

[3] A. Varga. “Balancing free square-root algorithm for computing singular perturbation approximations”. In: (1991).

[4] A. Stephen Morse. “Control Using Logic-Based Switching”. In: (1997).

[5] Kumpati S. Narendra and Jeyendran Balakrishnan. “Adaptive Control Using Multiple Models”. In: (1997).

[6] Zhe Lin. “Gain scheduling of aircraft pitch attitude and control of discrete, affine, linear parametrically varying systems”. In: (2002).

[7] M. Karpel, B. Moulin, and P. C. Chen. “Dynamic Response of Aeroservoelastic Systems to Gust Excitation”. In: *Journal of Aircraft* 42.5 (2005), pp. 1264–1272. ISSN: 0021-8669. DOI: 10.2514/1.6678.

[8] Andres Marcos, Subhabrata Ganguli, and Gary J Balas. “An application of H_∞ fault detection and isolation to a transport aircraft”. In: *Control Engineering Practice* 13.1 (2005), pp. 105–119.

[9] P. Apkarian and D. Noll. “Nonsmooth H ∞ Synthesis”. In: *IEEE Transactions on Automatic Control* 51.1 (2006), pp. 71–86. ISSN: 00189286. DOI: 10.1109/TAC.2005.860290.

[10] Sajjad Fekri, Michael Athans, and Antonio Pascoal. “Issues, progress and new results in robust adaptive control”. In: *International Journal of Adaptive Control and Signal Processing* 20.10 (2006), pp. 519–579. ISSN: 08906327. DOI: 10.1002/acs.912.

[11] Sigurd Skogestad and Ian Postlethwaite. *Multivariable feedback control: analysis and design*. Vol. 2. Citeseer, 2007.

[12] Christian Ballauf. *Dämpfung aeroelastischer Strukturen mit modelladaptiver Regelung: Zugl.: München, Techn. Univ., Diss., 2008*. Als Ms. gedr. Vol. 1155. Fortschrittberichte VDI Reihe 8, Mess-, Steuerungs- und Regelungstechnik. Düsseldorf: VDI-Verl., 2008. ISBN: 9783185155086.

[13] T Kier and G Looye. “Unifying Manoeuvre and Gust Loads Analysis”. In: *International Forum on Aeroelasticity and Structural Dynamics, No. IFASD-2009-106*. 2009.

[14] Ioan Doré Landau et al. *Adaptive Control*. London: Springer London, 2011. ISBN: 978-0-85729-663-4. DOI: 10.1007/978-0-85729-664-1.

[15] Timothy Josh Wheeler. “Probabilistic performance analysis of fault diagnosis schemes”. PhD thesis. UC Berkeley, 2011.

[16] Randal W Beard and Timothy W McLain. *Small unmanned aircraft: Theory and practice*. Princeton university press, 2012.

[17] J. Chen and R.J. Patton. *Robust Model-Based Fault Diagnosis for Dynamic Systems*. The International Series on Asian Studies in Computer and Information Science. Springer US, 2012. ISBN: 9781461551492.

[18] Elisa Capello, Giorgio Guglieri, and Fulvia Quagliotti. “L1 Adaptive Controller Design for Gust Load Alleviation”. In: (2014).

[19] Vladimir Hanta and Aleš Procházka. “Rational Approximation of Time Delay”. In: (2014).

[20] Bálint Vanek et al. “Bridging the gap between theory and practice in LPV fault detection for flight control actuators”. In: *Control Engineering Practice* 31 (2014), pp. 171–182.

[21] Andreas Knoblach. “Robust Performance Analysis for Gust Loads Computation”. In: (2015).

[22] Wen Fan, Hugh H. T. Liu, and Raymond H. S. Kwong. “Gain-Scheduling Control of Flexible Aircraft with Actuator Saturation and Stuck Faults”. In: *Journal of Guidance, Control, and Dynamics* 40.3 (2017), pp. 510–520. ISSN: 0731-5090. DOI: 10.2514/1.G002222.

[23] Andreas Varga. *Solving Fault Diagnosis Problems*. Vol. 84. Cham: Springer International Publishing, 2017. ISBN: 978-3-319-51558-8. DOI: 10.1007/978-3-319-51559-5.

[24] Yasser M Meddaikar et al. “Aircraft aeroservoelastic modelling of the FLEXOP unmanned flying demonstrator”. In: *AIAA Scitech 2019 Forum*. 2019, p. 1815.

[25] Daniel Ossmann and Manuel Pusch. “Fault Tolerant Control of an Experimental Flexible Wing”. In: *Aerospace* 6.7 (2019), p. 76.

[26] Béla Takarics and Bálint Vanek. “Tensor Product Model-based Robust Flutter Control Design for the FLEXOP Aircraft”. In: *IFAC-PapersOnLine* 52.12 (2019). 21st IFAC Symposium on Automatic Control in Aerospace ACA 2019, pp. 134–139.

[27] Manuel Pusch. *Blending of Inputs and Outputs for Modal Control of Aeroelastic Systems: Dissertation*. München: Verlag Dr. Hut, 2020. ISBN: 978-3-8439-4661-2.

[28] Charles Poussot-Vassal et al. “Interpolatory Methods for Generic BizJet Gust Load Alleviation Function”. In: (2021).

[29] Matthias Wuestenhagen et al. “Aeroservoelastic Modeling and Analysis of a Highly Flexible Flutter Demonstrator”. In: *2018 Atmospheric Flight Mechanics Conference*. Reston, Virginia: American Institute of Aeronautics and Astronautics, 6252018. ISBN: 978-1-62410-557-9. DOI: 10.2514/6.2018-3150.

[30] N. Aouf, B. Boulet, and R. Botez. “A gain scheduling approach for a flexible aircraft”. In: *Proceedings of the 2002 American Control Conference (IEEE Cat. No.CH37301)*. IEEE, 8.05.2002 - 10.05.2002, 4439–4442 vol.6. ISBN: 0-7803-7298-0. DOI: 10.1109/ACC.2002.1025347.

6 Annexes with additional information

This part might remain confidential and thus not be delivered.

The EC reviewer might ask for an insight – in this case a NDA is recommended.